The contribution of Micro-CT to the evaluation of trabecular bone at the posterior part of the auricular surface in men

Céline Deguette, Daniel Chappard, H. Libouban, Guillaume Airagnes, Clotilde Rougé-Maillart, Norbert Telmon

Int J Legal Med
DOI 10.1007/s00414-014-1139-1

TECHNICAL NOTE

The contribution of Micro-CT to the evaluation of trabecular bone at the posterior part of the auricular surface in men

Céline Deguette · Daniel Chappard · Hélène Libouban · Guillaume Airagnes · Clotilde Rouge-Maillart · Norbert Telmon

Received: 4 May 2014 / Accepted: 10 December 2014

Abstract
Aim Using multi-slice computed tomography (MSCT), Barrier et al. described the disappearance at the posterior auricular surface of a "central line" (CL) and "juxtalinear cells" (JLCs) belonging to a trabecular bundle, and a trabecular density gradient around the CL that decreased with age. The aim of our study was to use micro-CT to test these findings, referring to the concept of Ascadi and Nemeskeri.
Methodology The coxal bones of fifteen males were used; age was known. CLs were identified on MSCT-sections using Barrier's method (64 detectors, 0.6 mm slice thickness, 0.1 mm overlap) with two different software programs (Synapse®, Amira®). Then, CLs were researched on microCT slices (pixel size: 36 μm). Three volumes of interest were defined (around, above, and below CL), and 3D morphometric parameters of the trabecular microarchitecture (particularly BV/TV and DA) were calculated. Two-tailed statistical analyses were performed attempting to correlate these parameters with age at death.
Results CLs and JLCs were observed on micro-CT slices, but with moderate agreement between both imaging techniques. Their presence was not correlated with the age of the subjects. Around the CL, BV/TV decreased significantly with age; DA was negatively correlated with BV/TV and had a tendency to increase with age. Between areas above and below the CL, there was a BV/TV gradient and both BV/TVs decreased in parallel with age.
Conclusion Our findings regarding the contribution of micro-CT to the evaluation of trabecular bone could be a promising research approach for application in a larger study population.

Keywords Forensic science · Forensic anthropology · Trabecular bone · Age at death · MSCT · Micro-CT · Auricular surface

C. Deguette (✉) · C. Rouge-Maillart
CHU Angers, Department of Forensic Medicine, LUNAM Université, Angers Cedex, France
e-mail: celinedeguette@free.fr

C. Deguette · D. Chappard · H. Libouban · C. Rouge-Maillart
GEROM Groupe Etudes Remodelage Osseux et bioMatériaux, LUNAM Université, IRIS-IBS Institut de Biologie en Santé, CHU d'Angers, 49933 Angers Cedex, France

G. Airagnes
AP-HP, Department of Psychiatry, Hôpitaux Universitaires Paris Ouest, Paris, France

N. Telmon
Laboratoire Anthropologie Moléculaire et Imagerie de synthèse, Université Paul Sabatier, FRE 2960CNRS, Toulouse Cedex, France

N. Telmon
Department of Forensic Medicine, CHU Toulouse Rangueil, Toulouse Cedex, France

G. Airagnes
Faculté de Médecine, Université Paris Descartes, Sorbonne Paris Cité, Paris, France

Introduction

Determining as precisely as possible the age of a skeleton at time of death is a major issue in forensic practice. For adult skeletons, several approaches have been described, mainly based on macroscopic study of degenerative changes of articular surfaces, most commonly the auricular surface (AS) [1–3]. Nevertheless, some other researchers are focused on the study of trabecular bone. Trabecular bone consists of a network of trabeculae, organized in plates and pillars with an anisotropic distribution. These plates are disposed parallel to the mechanical forces acting on the bone (i.e., application of Wolf's law) [4, 5]. Plates are vertically disposed when submitted to uniaxial strains, as for vertebrae, and arciform organize into bundles when submitted to multiple strain directions, as for the femoral head and calcaneus [6]. Trabecular bundle structures have an

Published online: 24 December 2014

adaptative response to the changes in stress trajectories induced by several factors, such as exercise, mechanical loading, body mass increase, and physical behaviors [7–9]. Ascadi and Nemeskeri [10] proposed six age classification categories for the trabecular bundles, based on the gradual loss of the two major trabecular bundles at the upper femoral extremity, searched using X-ray images although these results were challenged by other studies working on osteoporosis.

The trabecular microarchitecture (TM) localized in the human pelvis has stress-influenced trabecular bundles [11–13]. Indeed, due to bipedalism, this area is an important load transfer point and constrains dispersal [14–16]. Two main trabecular bundles pass behind the AS, the ilio-ischiatic and the sacropubic bundles [11, 17]. The TM could be characterized by qualitative data, such as the degree of anisotropy (i.e., a preferred orientation of trabeculae), and by quantitative data, such as trabecular bone volume (BV/TV). Micro-CT allows a non-destructive study of trabecular bone microarchitecture in three dimensions with a resolution ranging from 5 to 15 micrometers [18].

Barrier et al. (2009) studied trabecular bone in the posterior part of the AS, which includes a sacropubic stress-influenced trabecular bundle, using multi-slice computer tomography (MSCT) [19]. They identified structures called the "central line" (CL) that could be surrounded or not by other structures called "juxtalinear cells" (JLCs), both of which followed the same direction as the sacropubic trabecular bundle. Interestingly, identification of these structures seemed to decrease with age. Moreover, an attenuation difference was observed on both sides of the CL for younger patients, whereas this gradient was lacking for the elderly. These findings could help develop another useful technique for learning about skeletal age at death, referring to the concept of Ascadi and Nemeskeri.

The aim of this preliminary study was to search for Barrier's findings using micro-CT, a modern imaging technique. Following Barrier's conclusions, we were inspired by the concept of Ascadi and Nemeskeri, without trying to exactly replicate the method of Ascadi and Nemeskeri itself. First, we searched for the CL and JLCs in the TM, using MSCT and micro-CT to compare the results. Second, we computed the trabecular bone microarchitecture parameters to search for an attenuation difference on both sides of the CL and for potential correlations with the age at death.

Material and methods

Bone collection

We used 15 dry coxal bones of males belonging to the University of Angers. Gender and age were known for all subjects thanks to DNA identification performed to confirm presumed identity following legal proceedings. Bones were split into three age categories as follows: 4 were between 30 and 40 years old, 6 were between 40 and 50, and five were older than 50.

MSCT procedure

Imaging was performed by a 64-detector General Electric OPTIMA CT 660 (at 140 kV, 200 mA, and a 20-mm FoV) with a slice thickness of 0.6 mm and a 0.1-mm overlap. Bones were placed in the same orientation, external surface downward. We used multiplanar reconstructions (MPR) on the ADWA software (General Electric) and volume rendering reconstruction (VRT).

Determination of the area of interest with MSCT slices

MPR reconstructions were used to localize the CL and JLCs, which are most frequently seen in the antero-posterior direction. MPR reconstructions were oriented perpendicularly to the AS (i.e., coronal slice in anatomic position). Then, slices were read one by one in the antero-posterior direction to bring out the slice in which the CL and/or JLCs could be identified (Fig. 1). This procedure was repeated with two different software programs *(SYNAPSE® (Fujifilm, USA) and AMIRA® (Mercury Computer System TGS);* image files (.dicom)*)* to prevent for potential software biases. In fact, the CL and JLCs were found between 65 and 90 % of the length of the AS with both software programs. This parallelepipedic volume defined the antero-posterior limits of our region of interest (ROI), providing a reproducible area whatever the length of the AS and which could be used even without the CL or JLCs.

Micro-CT procedure

Contrary to MSCT, micro-CT does not allow the study of entire coxal bone. The AS has to be cut from the entire bone in its full thickness with a scroll saw at an average distance from the AS between 2 and 5 mm. For micro-CT analysis, bone sample was affixed on the recipient aluminum bed with plasticine and examined with a Skyscan 1076 microCT (Bruker microCT, Kontich, Belgium). Samples were all placed with the medial side upward and the posterior area in the front of the X-ray tube. The beginning of the AS was localized with a metal wire. A scout scan allowed localizing the ROI in the antero-posterior direction as defined previously via MSCT. Projection images were obtained at 80 kV and 100 μA, with a 1-mm aluminum filter and a pixel size of 36 microns. An angle rotation of 0.2° on 180° was used between each image acquisition. Images were automatically stored in .tif format until reconstruction in a stack of 2D sections in .bmp format with indexed grey levels with the Nrecon software (Bruker). Reconstructed 3D models were obtained from the 2D sections by surface rendering software and 3D

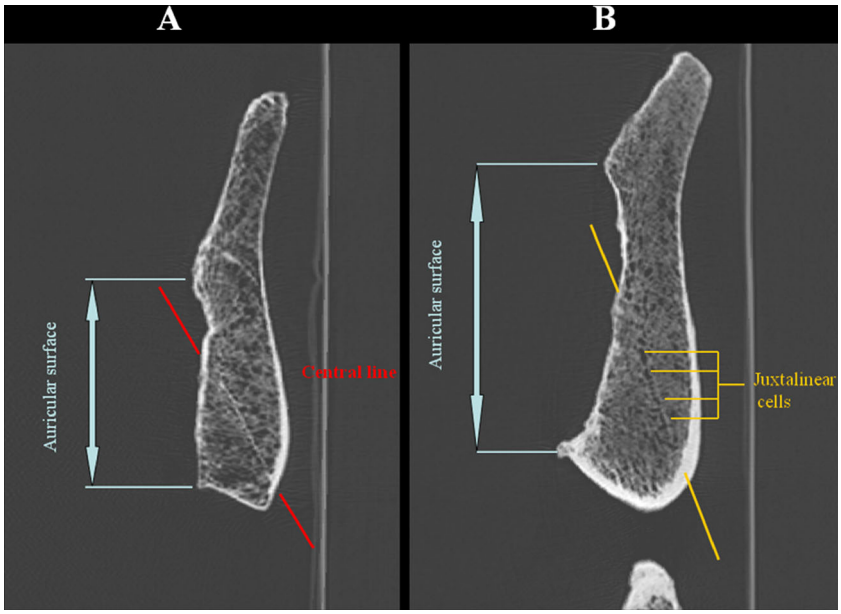

Fig. 1 **a** "Central line" displayed on an MSCT slice; **b** "Juxtalinear cells" displayed on an MSCT slice

measurements with CtAn software (release 1.13, Bruker). The ROI was adjusted in the vertical direction by interactively drawing polygons on the 2D images before reconstruction. Limits of the polygons were the upper and the lower limits of the AS. Only a few polygons needed to be drawn (~ one every 50 slices) and the intermediary ones were calculated by software interpolation. 3D reconstructions with volume rendering were performed for each sample, using CTVox V2.2 software (Bruker) to check the limits of the ROI.

Presence or absence of the CL and a scale-like trabecular scaffold corresponding to the JLCs, as their localization in the anterior posterior direction, were searched on all the stacks of 2D images once and then two weeks later by the same investigator. To avoid confusion with the histological nomenclature, the term "juxtalinear cells" will be substituted by "trabecular scale" (TS), which is a more descriptive and anatomical term.

Localization of these "trabecular structures" (CL or TS) in bone thickness has been achieved thanks to three landmarks on several 2D sections for each bone. This procedure was assisted by CtAn software that computes the distance between the trabecular structures and the endosteum of the AS (Fig. 2).

From these data, three trabecular volumes of interest (VOI) (Fig. 3) were defined as follows: below the CL (VOI 1); above the CL or its supposed position (VOI 2); and around the CL (VOI 3). VOI 1 and VOI2 were designed by drawing interactively polygons on the 2D images, excluding cortical bone (by

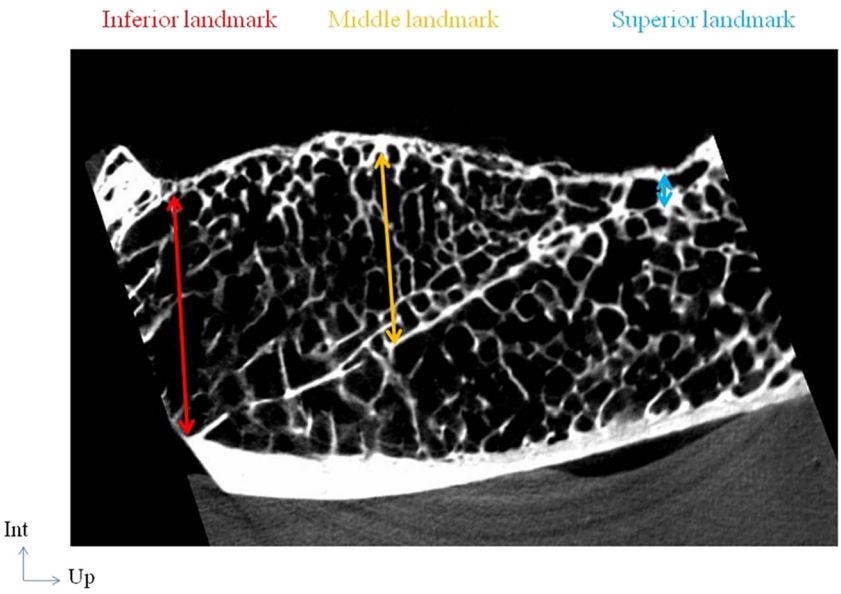

Fig. 2 Localization of the three landmarks

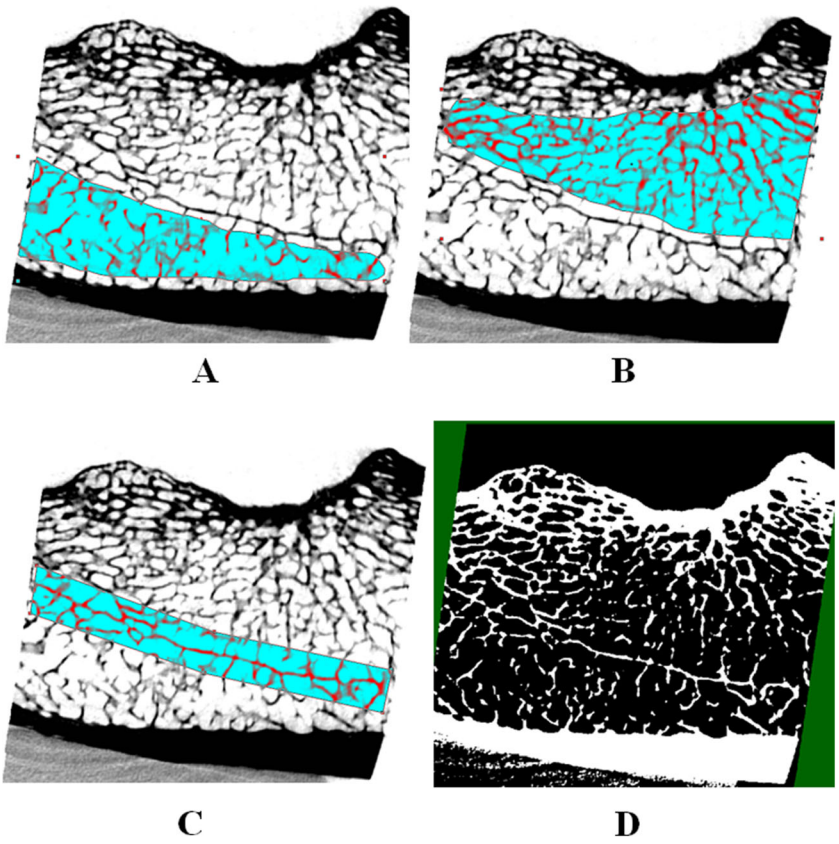

Fig. 3 **a** VOI 1: Area infra "central line"; **b** VOI 2: Area supra "central line"; **c** VOI 3: Area around the "central line"; **d** Binarized images

cutting the trabeculae from the endosteal side of the cortices) and the CL. Finally, images initially as a distribution of gray levels were binarized to become black or white pixels by using an interactive threshold. Black pixels refer to marrow spaces while white pixels refer to trabeculae. Trabecular bone microarchitecture parameters were computed from these images.

Morphometric parameters for description of trabecular bone microarchitecture

Morphometric analysis was done on the stacks of our 2D binarized slices. Standard bone histomorphometric nomenclatures, symbols, and units were used as described in the report of the American Society for Bone and Mineral Research [20]: Trabecular Bone Volume (BV/TV, expressed in %): it represents the fraction volume of the VOI occupied by trabeculae; Trabecular thickness (Tb.Th in μm) [21]; Trabecular number (Tb.N in 1/mm); Trabecular separation(Tb.Sp in μm); Structure model index (SMI) [21, 22]; Trabecular Bone Pattern factor ($Tb.P_f$) [23]; Degree of anisotropy (DA). Anisotropy is the property of having a preferential alignment of structures in 3D analysis (here, the trabeculae), as opposed to isotropy, which implies identical properties in all directions. DA is measured by a mean intercept length (MIL) analysis. With CtAn, DA is 0 for total isotropy and 1 for total anisotropy.

Statistical analysis

SPSS software 16.0 (SPSS, Chicago, Illinois) and Systat 13 (Systat Inc. San José, MA) were used. Descriptive analyses were presented in terms of mean, standard deviation, and median.

Agreement between MSCT and micro-CT for identifying "trabecular structures" was measured with a Cohen's Kappa test (strong agreement was defined as >80 %). A nonparametric Kruskal Wallis test was used to search for significant differences between age categories. To examine correlations between the first and second observations of anterior and posterior limits of trabecular structures on 2D images with microCT, we used the nonparametric Spearman test. For each trabecular parameter, the difference (Δ) between VOI 1 and VOI 2 was computed as follows: Δ=parameter of VOI 2 – parameter of VOI 1. Nonparametric Spearman tests were also used to examine the following: 1) correlations

between age and successively VOI 1, VOI 2, and VOI 3; 2) correlations between VOI 1 and VOI 2; and 3) correlations between age and each delta (Δ). For all statistical analysis, tests were two-tailed and the significance level was set at 5 % ($p<0.05$).

Results

Localization of "trabecular structures" and histological identification

Intra-observer stability identifying the localization of anterior and posterior limits of "trabecular structures," showed good test-retest reliability with respective correlations of 0.565 ($p=0.028$) and 0.736 ($p=0.002$).

Nine samples had continuous and well visible TSs or CLs as per micro-CT examination. For these samples, localization of the landmarks were similar; these landmarks were used to determine areas of interest for the entire cohort (see Table 1). Observed CLs were trabeculae organized in plates, always localized in the same area and going in the same direction. In fact, CLs began at the upper limit of the rear of the anterior part of the AS and were going down to the external face of the coxal bone, in the acetabular area. Observed TSs were localized in the same area as the CLs. They were organized in plates and in pillars that crossed themselves, building medullar cavities approximately rectangular with a main axis following the plate's direction.

Comparisons between MSCT and with micro-CT observations

We found a moderate agreement between findings using MSCT and micro-CT 2D-section observations ($\kappa=0.59$) (see Table 2).

With MSCT, the observed mean age differences between subjects for which a CL, TS, or neither was not seen did not reach significance ($K=5.144$; $p=0.076$). However, with micro-CT, observed mean age differences between these three groups became significant ($K=6.827$; $p=0.033$): subjects with an observed TS (40.4±5.1 y.o.) were younger than those with an observed CL (47.7±10.3 y.o.). The oldest were those without observed "trabecular structures" (59.6±2.8 y.o.).

Table 1 The three landmarks for the "central line" or "trabecular scale" locations

Location (%)[a]	Inferior landmark[b]	Middle landmark	Superior landmark
Mean	69.70 %	48 %	14.50 %
Standard deviation (SD)	±8.5 %	±7.9 %	±7.1 %
Median	72.18 %	48.68 %	13.05 %

[a] height between the auricular surface and the landmark/height of trabecular bone (see Fig. 2)

[b] located at the bottom of the sample

Table 2 "Trabecular structures" visually evaluated on MSCT and micro-CT pictures

Class of age	Name of sample	MSCT pictures	Micro-CT pictures
30–40 y.o.	CA 01	CL[a]	TS[c]
	CA 08	JLC[b]	TS
	CA 24	CL	CL (+ TS)
	CA 29	CL	CL (+ TS)
40–50 y.o.	CA 03	JLC	CL (+ TS)
	CA 04	JLC	CL (+ TS)
	CA 10	CL	TS
	CA 25	JLC	TS
	CA 30	JLC	TS
	CA 38	CL	CL+TS
50–60 y.o.	CA 16	0[d]	0
	CA 27	JLC	CL (+ TS)
	CA 33	CL	CL (+ TS)
60–70 y.o.	CA 26	0	0
	CA 32	0	0

[a] *CL* "central line"

[b] *JLC* "juxtalinear cells" without "central line"

[c] *TS* "trabecular scale"

[d] 0: no visually detectable trabecular structure

Analysis for trabecular bone microarchitecture parameters and for their correlations with the age at death

Means, medians, and standard deviations of trabecular parameters are summarized, respectively, for VOI 1, VOI 2, and VOI 3 in Table 3, Table 4, and Table 5. Correlations between age and trabecular bone microarchitecture parameters of VOI 1, VOI 2 and VOI 3 are presented in Table 6. Correlations between DA and trabecular bone parameters of VOI 1, VOI 2, and VOI 3 are presented in Table 7. Results concerning differences between VOI 1 and VOI 2 (Δ) are presented in Table 8. Finally, correlations between the trabecular bone microarchitecture parameters of VOI 1 and VOI 2 are presented in Table 9.

Discussion

The aim of this preliminary study was to search for the findings of Barrier et al. (2009) at the microarchitecture level using micro-CT, referring to the concept of Ascadi and Nemeskeri.

Table 3 Descriptive analysis of VOI 1 parameters according to age

		BV/TV	$Tb.P_f$	SMI	Tb.Th	Tb.N	Tb.Sp	DA
30–40 y.o.	Mean	16.602	3.175	1.718	0.277	599	1004	0.924
	Standard deviation	2.0186	0.243	0.029	0.018	43	83	0.038
	Median	16.586	3.223	1.726	0.274	598	991	0.916
40–50 y.o.	Mean	13.282	3.702	1.878	0.285	472	1211	0.917
	Standard deviation	3.457	0.741	0.257	0.032	142	232	0.080
	Median	14.961	3.559	1.852	0.276	492	1099	0.931
>50 y.o.	Mean	10.729	4.296	2.101	0.316	341	1413	0.928
	Standard deviation	4.762	1.409	0.479	0.042	141	138	0.064
	Median	8.825	4.667	2.169	0.300	311	1446	0.935

Table 4 Descriptive analysis of VOI 2 parameters according to age

		BV/TV	$Tb.P_f$	SMI	Tb.Th	Tb.N	Tb.Sp	DA
30–40 y.o.	Mean	20.602	2.704	1.623	0.308	667	875	0.732
	Standard deviation	3.179	0.683	0.152	0.032	51	40	0.118
	Median	20.931	2.611	1.555	0.301	691	872	0.722
40–50 y.o.	Mean	15.038	3.797	1.924	0.302	494	1104	0.788
	Standard deviation	4.505	0.916	0.192	0.042	117	239	0.139
	Median	15.363	3.717	1.928	0.301	537	993	0.812
>50 y.o.	Mean	14.811	3.550	1.916	0.324	453	1280	0.738
	Standard deviation	6.607	1.228	0.356	0.021	195	347	0.167
	Median	15.363	3.717	1.928	0.301	537	993	0.812

For all bones for which a CL or TS were observed, these "trabecular structures" were both localized in the same area. Moreover, plates were oriented in the same direction on MSCT and on micro-CT images ; from the rear of the AS to the acetabular region. These structures are, therefore, an integral part of the sacroiliac bundle described by Correnti [11] who observed that plates followed the direction of the main mechanical constraint force. Even localization was the same with the two imaging techniques; the types of "trabecular structures" were different in a third of the cases. This difference could be explained by a gap of image resolution; micro-CT had a resolution of 36 microns in this study, allowing for a more accurate observation of these structures, like early changes in the microarchitecture or when CL was very discontinuous, which could not be noticed on thicker sections with the MSCT (600 μm) [24]. Moreover, several independent trabeculae could be observed combined in a single slice imitating a CL due to a projection effect [25]. The semi-fractal organization of trabecular bone and the resolution of the image in voxels could also affect the determination of bone parameters and the accuracy of bony structure identification [26, 27]. We have not performed an inter-observer reliability

Table 5 Descriptive analysis of VOI 3 parameters according to age

		BV/TV	$Tb.P_f$	SMI	Tb.Th	Tb.N	Tb.Sp	DA
30–40 y.o.	Mean	22.059	7.706	1.249	0.305	721	936	0.708
	Standard deviation	3.263	11.782	0.135	0.026	49	53	0.102
	Median	22.274	2.111	1.269	0.306	726	923	0.728
40–50 y.o.	Mean	17.844	2.472	1.517	0.305	586	1051	0.769
	Standard deviation	3.021	0.508	0.148	0.037	071	84	0.209
	Median	17.159	2.644	1.566	0.29	600	1034	0.880
>50 y.o.	Mean	12.793	3.687	1.932	0.316	402	1292	0.919
	Standard deviation	3.945	0.983	0.304	0.017	111	103	0.031
	Median	11.806	3.896	2.046	0.322	360	1307	0.909

Table 6 Correlations table between age and trabecular bone microarchitecture parameters of VOI 1, VOI 2, and VOI 3

	Age		
Trabecular bone microarchitecture parameters	VOI 1	VOI 2	VOI 3
BV/TV	$r=-0.535$, $p=0.040$	$r=-0.302$, $p=0.174$	$r=-0.719$, $p=0.003$
Tb.Th	$r=0.475$, $p=0.073$	$r=0.322$, $p=0.242$	$r=0.289$, $p=0.296$
Tb.N	$r=-0.696$, $p=0.004$	$r=-0.459$, $p=0.085$	$r=-0.880$, $p<0.001$
Tb.Sp	$r=0.766$, $p=0.001$	$r=0.667$, $p=0.007$	$r=0.887$, $p<0.001$
$Tb.P_f$	$r=0.475$, $p=0.073$	$r=0.141$, $p=0.616$	$r=0.399$, $p=0.140$
SMI	$r=0.506$, $p=0.054$	$r=0.381$, $p=0.161$	$r=0.838$, $p<0.001$
DA	$r=0.049$, $p=0.863$	$r=0.132$, $p=0.639$	$r=0.640$, $p=0.010$

Table 7 Correlations table between DA and other trabecular bone parameters of VOI 1, VOI 2, and VOI 3

	DA		
Trabecular bone microarchitecture parameters	VOI 1	VOI 2	VOI 3
BV/TV	$r=0.307$, $p=0.265$	$r=0.089$, $p = 0.752$	$r=-0.664$, $p=0.007$
Tb.Th	$r=0.029$, $p=0.919$	$r=-0.336$, $p=0.221$	$r=-0.121$, $p=0.666$
Tb.N	$r=0.139$, $p=0.621$	$r=0.214$, $p=0.443$	$r=-0.661$, $p=0.007$
Tb.Sp	$r=-0.121$, $p=0.666$	$r=-0.150$, $p=0.594$	$r=0.679$, $p=0.005$
$Tb.P_f$	$r=-0.232$, $p=0.405$	$r=-0.096$, $p=0.752$	$r=0.500$, $p=0.058$
SMI	$r=-0.311$, $p=0.260$	$r=-0.271$, $p=0.328$	$r=0.604$, $p=0.017$

test to search for these "trabecular structures" with both imaging techniques, something that could have given more strength to our results.

3D study focused on the sacroiliac bundle (VOI 3) showed a strong correlation between trabecular parameters and the age at death, higher than for VOI 1 or VOI 2. BV/TV decreased with age due to the decrease of Tb.N and the increase of Tb.Sp [6, 28–31]. Moreover, DA in VOI3 area significantly increased with age and was also significantly correlated with the decrease of BV/TV and Tb.N. These results are in agreement with previous findings; indeed, we already know that trabeculae are perforated or entirely destroyed over time, even with male subjects [30, 32–36]. These mechanisms concern preferentially trabeculae that are perpendicular or transverse to the main direction of the load, therefore, also perpendicular or transverse to the stress bundle [6, 30, 37]. Visual observation of a discontinuity or of disappearance of the CL after age 50 with MSCT cannot be explained by changes in trabecular

Table 8 Descriptive analysis between age and each Δ

		Δ BV/TV	Δ $Tb.P_f$	Δ SMI	Δ Tb.Th	Δ Tb.N	Δ Tb.Sp	Δ DA
30–40 y.o.	Mean	3.999	-0.471	-0.094	0.031	69	−129	-0.192
	Standard deviation	1.280	0.474	0.149	0.016	42	58	0.083
	Median	4.345	-0.612	-0.154	0.031	55	−139	-0.193
40–50 y.o.	Mean	1.757	0.095	0.046	0.016	22	−107	-0.129
	Standard deviation	2.834	0.795	0.211	0.028	62	73	0.167
	Median	1.736	0.021	-0.006	0.008	39	−107	-0.079
>50 y.o.	Mean	4.082	-0.746	-0.185	0.008	112	−132	-0.189
	Standard deviation	5.282	1.045	0.314	0.061	119	285	0.112
	Median	1.736	0.021	-0.006	0.008	39	−107	-0.079

Table 9 Correlation table between VOI 1 and VOI 2

VOI 1	VOI 2						
	BV/TV_2	Tb.Th_2	Tb.N_2	Tb.Sp_2	$Tb.P_f$_2	SMI_2	DA_2
BV/TV_1	r=0.729	r=0.118	r=0.718	r=−0.836	r=-0.650	r=−0.771	r=0.050
	p=0.002	p=0.676	p=0.003	p<0.001	p=0.009	p=0.001	p=0.860
Tb.Th_1	r=−0.068	r=0.550	r=−0.296	r=0.393	r=−0.071	r=0.136	r=0.200
	p=0.810	p=0.034	p=0.283	p=0.147	p=0.800	p=0.630	p=0.475
Tb.N_1	r=0.668	r=−0.136	r=0.746	r=-0.900	r=−0.529	r=−0.729	r=0.132
	p=0.007	p=0.630	p=0.001	p<0.001	p=0.043	p=0.002	p=0.639
Tb.Sp_1	r=−0.614	r=−0.018	r=−0.661	r=0.811	r=0.471	r=0.614	r=0.182
	p=0.015	p=0.950	p=0.007	p<0.001	p=0.076	p=0.015	p=0.516
$Tb.P_f$_1	r=−0.718	r=0.014	r=−0.757	r=0.857	r=0.629	r=0.786	r=−0.214
	p=0.003	p=0.960	p=0.001	p<0.001	p=0.012	p=0.001	p=0.443
SMI_1	r=−0.550	r=0. 225	r=−0.654	r=0.796	r=0.446	r=0.664	r=−0.364
	p=0.034	p=0.420	p=0.008	p<0.001	p=0.095	p=0.007	p=0.182
DA_1	r=0.157	r=0.075	r=0.211	r=−0.132	r=−0.211	r=−0.268	r=0.461
	p=0.576	p=0.791	p=0.451	p=0.639	p=0.451	p=0.334	p=0.084

bundle orientation, neither by a preferential destruction of the trabecular bundle. It is likely that 2D imaging interpretation, either with MSCT or with micro-CT, is not representative of trabecular bone microarchitectural organization in 3D.

Analysis of MSCT slices previously found a visual gradient of density that may disappear over time [19]. We searched for this gradient as the visual translation of changes in DA or in BV/TV. In our study, although there was a gradient of anisotropy between the two sides of the CL (VOI 1 area was more anisotropic than VOI 2), the DA of VOI 1, of VOI 2, and ΔDA were not correlated with the age at death. In other words, the anisotropy gradient does not disappear over time and we cannot learn the age at death. BV/TV of the VOI 1 area was significantly correlated with the age at death due to the same mechanism of trabeculae perforation as described for the VOI 3 area. Only in the VOI 2 area, did this correlation reach significance. That could be explained by the difficulty in defining the upper limit of trabecular bone in the VOI 2 area, which is close to the subchondral area, known to generate "trabecularization of cortices" or "trabecular corticalization" [38], making limits unclear between trabecular and cortical bones.

BV/TV in the VOI 1 area, as with BV/TV in the VOI 2 area, correlate with the age at death. We also observed a strong correlation between the BV/TV of these two areas, meaning that bone loss had similarly interesting VOI 1 and VOI 2 areas. This finding rules out the hypothesis that the visual disappearance of the density gradient described via MSCT could be due to changes in the BV/TV gradient [19]. Another potential explanation of the lack of agreement between 2D MSCT and 3D micro-CT analysis is that working with 2D sections greater than 500 μm focuses on the texture of the bone rather than the microarchitectural network itself [6, 17, 25, 39]. Nevertheless, several studies have shown good association between texture analysis of MSCT sections and 3D microarchitecture analyzed with micro-CT [40–43]. Moreover, cortices and "cortical trabecularization" underlying the AS could also induce a parasite texture on the resulting image [40], responsible for poor visual interpretation. Finally, visual analysis of "density" is difficult to interpret and cannot be associated with trabecular microarchitectural features.

Since determining the age at death is a major issue in forensic medicine, our findings regarding the contribution of micro-CT to the evaluation of trabecular bone could be a promising research approach. This preliminary study on a few male samples from a modern forensic collection needs to be extended in a larger collection more representative of the general population, including female samples.

References

1. Buckberry JL, Chamberlain AT (2002) Age estimation from the auricular surface of the ilium: a revised method. Am J Phys Anthropol 119:231–239
2. Lovejoy CO, Meindl RS, Pryzbeck TR, Mensforth RP (1985) Chronological metamorphosis of the auricular surface of the ilium: a new method for the determination of adult skeletal age at death. Am J Phys Anthropol 68:15–28
3. Rougé-Maillart C, Vielle B, Jousset N, Chappard D, Telmon N, Cunha E (2009) Development of a method to estimate skeletal age at death in adults using the acetabulum and the auricular surface on a Portuguese population. Forensic Sci Int 188:91–95
4. Wolff J (1892) Das Gesetz der Transformation des Knochen. Hirschwald Verlag, Berlin

5. Pontzer H, Lieberman DE, Momin E, Devlin MJ, Polk JD, Hallgrimsson B, Cooper DM (2006) Trabecular bone in the bird knee responds with high sensitivity to changes in load orientation. J Exp Biol 209:57–65
6. Chappard D, Baslé MF, Legrand E, Audran M (2008) Trabecular bone microarchitecture: a review. Morphologie 92:162–170
7. Lai YM, Qin L, Yeung HY, Lee KK, Chan KM (2005) Regional differences in trabecular BMD and micro-architecture of weight-bearing bone under habitual gait loading–a pQCT and microCT study in human cadavers. Bone 37:274–282
8. Ryan TM, Ketcham RA (2005) Angular orientation of trabecular bone in the femoral head and its relationship to hip joint loads in leaping primates. J Morphol 265:249–263
9. Barak MM, Lieberman DE, Hublin JJ (2011) A Wolff in sheep's clothing: trabecular bone adaptation in response to changes in joint loading orientation. Bone 49:1141–1151
10. Acsadi G, Nemeskeri L (1970) History of human life span and mortality. Akademiai Kiado, Budapest
11. Correnti V (1955) la basi morfomeccaniche della structtura dell'osso iliaco. Riv Antrop 289–336.
12. Dalstra M, Huiskes R (1995) Load transfer across the pelvic bone. J Biomech 28:715–724
13. Versier G (2009) Physiologie de la sacro-iliaque. Rev Rhum 76:734–740
14. Martinon-Torres M (2003) Quantifying trabecular orientation in the pelvic cancellous bone of modern humans, chimpanzees, and the Kebara 2 Neanderthal. Am J Hum Biol 15:647–661
15. Rook L, Bondioli L, Kohler M, Moya-Sola S, Macchiarelli R (1999) Oreopithecus was a bipedal ape after all: evidence from the iliac cancellous architecture. Proc Natl Acad Sci U S A 96:8795–8799
16. Tobias PV (1998) Ape-like australopithecus after seventy years: was it a hominid? J R Anthropol Inst 4:283–308
17. Lespessailles É, Chappard C, Bonnet N, Benhamou CL (2006) Imagerie de la microarchitecture osseuse. Rev Rhum 73:435–443
18. Muller R, Van Campenhout H, Van Damme B, Van Der Perre G, Dequeker J, Hildebrand T, Ruegsegger P (1998) Morphometric analysis of human bone biopsies: a quantitative structural comparison of histological sections and micro-computed tomography. Bone 23:59–66
19. Barrier P, Dedouit F, Braga J, Joffre F, Rouge D, Rousseau H, Telmon N (2009) Age at death estimation using multislice computed tomography reconstructions of the posterior pelvis. J Forensic Sci 54:773–778
20. Dempster DW, Compston JE, Drezner MK, Glorieux FH, Kanis JA, Malluche H, Meunier PJ, Ott SM, Recker RR, Parfitt AM (2013) Standardized nomenclature, symbols, and units for bone histomorphometry: a 2012 update of the report of the ASBMR Histomorphometry Nomenclature Committee. J Bone Miner Res 28: 2–17
21. Hildebrand T, Ruegsegger P (1997) A new method for the model-independent assessment of thickness in three-dimensional images. J Microsc 185:67–75
22. Laib A, Kumer JL, Majumdar S, Lane NE (2001) The temporal changes of trabecular architecture in ovariectomized rats assessed by MicroCT. Osteoporos Int 12:936–941
23. Link TM, Majumdar S, Konermann W, Meier N, Lin JC, Newitt D, Ouyang X, Peters PE, Genant HK (1997) Texture analysis of direct magnification radiographs of vertebral specimens: correlation with bone mineral density and biomechanical properties. Acad Radiol 4: 167–176
24. Jiang Y, Zhao JJ, Mitlak BH, Wang O, Genant HK, Eriksen EF (2003) Recombinant human parathyroid hormone (1–34) [teriparatide] improves both cortical and cancellous bone structure. J Bone Miner Res 18:1932–1941
25. Benhamou CL, Pothuaud L, Lespessailles E (2000) Caractérisation de la microarchitecture trabéculaire osseuse par analyse de texture. ITBM-RBM 21:351–358
26. Isaksson H, Toyras J, Hakulinen M, Aula AS, Tamminen I, Julkunen P, Kroger H, Jurvelin JS (2011) Structural parameters of normal and osteoporotic human trabecular bone are affected differently by microCT image resolution. Osteoporos Int 22:167–177
27. Kim DG, Christopherson GT, Dong XN, Fyhrie DP, Yeni YN (2004) The effect of microcomputed tomography scanning and reconstruction voxel size on the accuracy of stereological measurements in human cancellous bone. Bone 35:1375–1382
28. Chappard C, Marchadier A, Benhamou CL (2008) Side-to-side and within-side variability of 3D bone microarchitecture by conventional micro-computed tomography of paired iliac crest biopsies. Bone 43: 203–208
29. Fazzalari NL, Parkinson IH (1998) Femoral trabecular bone of osteoarthritic and normal subjects in an age and sex matched group. Osteoarthritis Cartilage 6:377–382
30. Parfitt AM, Mathews CH, Villanueva AR, Kleerekoper M, Frame B, Rao DS (983) Relationships between surface, volume, and thickness of iliac trabecular bone in aging and in osteoporosis. Implications for the microanatomic and cellular mechanisms of bone loss. J Clin Invest 72:1396–1409.
31. Ding M, Odgaard A, Hvid I (2003) Changes in the three-dimensional microstructure of human tibial cancellous bone in early osteoarthritis. J Bone Joint Surg 85-B
32. Szulc P, Munoz F, Duboeuf F, Marchand F, Delmas PD (2005) Bone mineral density predicts osteoporotic fractures in elderly men: the MINOS study. Osteoporos Int 16:1184–1192
33. Bouvard B, Hoppe E, Chappard D, Audran M (2010) Ostéoporose masculine. Encycl Med Chir App Locom (pp. FASC. 14062 A14010.).
34. Homminga J, McCreadie BR, Ciarelli TE, Weinans H, Goldstein SA, Huiskes R (2002) Cancellous bone mechanical properties from normals and patients with hip fractures differ on the structure level, not on the bone hard tissue level. Bone 30:759–764
35. Ciarelli TE, Fyhrie DP, Schaffler MB, Goldstein SA (2000) Variations in three-dimensional cancellous bone architecture of the proximal femur in female hip fractures and in controls. J Bone Miner Res 15:32–40
36. Cortet B, Marchandise X (2001) Bone microarchitecture and mechanical resistance. Joint Bone Spine 68:297–305
37. Newitt DC, Majumdar S, van Rietbergen B, von Ingersleben G, Harris ST, Genant HK, Chesnut C, Garnero P, MacDonald B (2002) In vivo assessment of architecture and micro-finite element analysis derived indices of mechanical properties of trabecular bone in the radius. Osteoporos Int 13:6–17
38. Zebaze RM, Seeman E (2005) Cortical stability of the femoral neck and hip fracture risk. Lancet 366:1523, author reply 1524–1525
39. Guggenbuhl P, Chappard D, Garreau M, Bansard JY, Chales G, Rolland Y (2008) Reproducibility of CT-based bone texture parameters of cancellous calf bone samples: influence of slice thickness. Eur J Radiol 67:514–520
40. Guggenbuhl P, Bodic F, Hamel L, Basle MF, Chappard D (2006) Texture analysis of X-ray radiographs of iliac bone is correlated with bone micro-CT. Osteoporos Int 17:447–454
41. Diederichs G, Link T, Marie K, Huber M, Rogalla P, Burghardt A, Majumdar S, Issever A (2008) Feasibility of measuring trabecular bone structure of the proximal femur using 64-slice multidetector computed tomography in a clinical setting. Calcif Tissue Int 83:332–341
42. Diederichs G, Link TM, Kentenich M, Schwieger K, Huber MB, Burghardt AJ, Majumdar S, Rogalla P, Issever AS (2009) Assessment of trabecular bone structure of the calcaneus using multi-detector CT: correlation with microCT and biomechanical testing. Bone 44:976–983
43. Bauer JS, Issever AS, Fischbeck M, Burghardt A, Eckstein F, Rummeny EJ, Majumdar S, Link TM (2004) Multislice-CT for structure analysis of trabecular bone - a comparison with micro-CT and biomechanical strength. Röfo 176:709–718